

FEDSM-ICNMM2010-305- (

NUMERICAL INVESTIGATION OF FLUID FLOW INSIDE THE POROUS MEDIUM OF GDL

Mehdi Shahraeeni

School of Engineering
University of British Columbia Okanagan
Kelowna, BC V1V 1V7
Email: mehdi.shahraeeni@ubc.ca

Mina Hoorfar*

School of Engineering
University of British Columbia Okanagan
Kelowna, BC V1V 1V7
Email: mina.hoorfar@ubc.ca

ABSTRACT

A pore-network model is developed to study numerically the transient flow of fluid through the gas diffusion layer (GDL) of the PEM fuel cell. It is shown that the agglomeration of water droplet on the interface of the GDL and catalyst layer occurs faster for the samples with smaller pore diameters and lower contents of the hydrophobic agent. The study suggests that analysis of the temporal response of the GDL is a useful tool to evaluate its performance against transporting liquids.

NOMENCLATURE

l Throat length.
 i Current density, A/cm^2 .
 t^* Dimensionless time.
 z^* Dimensionless distance.
 V Cell voltage.
 E_{oc} Open circuit voltage.
 Ca Capillary number, $\mu V/\gamma$.
 M Mobility ratio, M_1/M_2 .
 f Hydrophilic fraction.
 θ_c Average contact angle.
 θ_{HI} Hydrophilic contact angle.
 θ_{HO} Hydrophobic contact angle.
 d_{avg} Average pore diameter.

INTRODUCTION

The agglomeration of liquid water on the interface of the catalyst layer (CL) and the gas diffusion layer (GDL) limits the efficiency of the proton exchange membrane (PEM) fuel cells. Especially, when the cell is working at high current densities, the rate of water production exceeds the rate at which water is removed from the CL. Several studies have been conducted to address the flooding phenomenon both experimentally and numerically [1-7]. In-situ measurements mostly consider the effects of GDL characteristics on the total efficiency of the cell [7-9]; while ex-situ visualization of liquid water motion inside the GDL helps to understand the details of phenomena underlying in flooding [2]. The ex-situ modeling deals with correlating the characteristics of liquid water flow inside the GDL, i.e. the saturation level and capillary pressure, to the performance of the porous material in transporting the liquid phase from the catalyst layer to the gas channel [10-17]. It is well established in the literature that the performance of the GDL is enhanced by adding a microporous layer to the GDL [13, 18], treating the GDL with a hydrophobic agent, and using a GDL with a larger pore size distribution [14-16, 19].

Recently, Park and Popov [19] proposed an analytical expression for studying the effect of the hydrophobic and structural properties of the cathode gas diffusion layer on mass transport in the PEM fuel cell. Their model suggests that GDLs with the largest average pore diameter and lowest hydrophilic fraction achieve highest current density. Since adding the hydrophobic agent reduces the average pore diameter [19], the two variables

*Address all correspondence to this author.

(i.e., the average pore diameter and hydrophilic fraction) are correlated to obtain the optimum values for these variables. They provided the saturation profiles across the GDL for various pairs of the average pore diameter and fraction of hydrophilic surface at the steady state condition. This motivated us to develop a pore-network model to investigate the transient response and details of water motion inside the GDL with different pore-size distributions and hydrophilic fractions. Using the model, the evolution of saturation profile versus time is obtained and analyzed.

NUMERICAL MODEL

The porous medium of the gas diffusion layer (GDL) is represented by a regular network of pores interconnected via throats. The geometric specifications of the network are determined with respect to porosimetry data available for E-TEK carbon paper [19]. To study the effect of the variation of the pore diameter on the water motion pattern, three different average pore diameters of $d_{avg} = 2, 4$ and $6\mu m$ are considered. The diameters of the pores are uniformly distributed in the network within 5% of the average pore diameter. Throats are considered as small capillary tubes along which the pores are connected together. The diameter of the throat which determines the conductance of the flow is considered as half of the average pore diameter ($d_{throat} = d_{avg}/2$). The length of the throat is assumed to be constant in the regular network ($l = 20\mu m$). The characteristics of the network are presented in Table 1.

TABLE 1. PARAMETERS OF PORE-NETWORK.

Parameter	Value	Parameter	Value
Pore Diameter	2, 4, 6 μm	Throat Diameter	1, 2, 3 μm
Coordination Number	6	Throat Length	20 μm
Mesh Size	20 \times 20 \times 20	Hydrophilic Fraction	0.4, 0.5, 0.6
Surface Tension (σ)	0.0635 J/m ²	Current Density	1.0 A/cm ²
Hydrophilic CA	50° – 80°	Hydrophobic CA	100° – 125°
Air Viscosity	1.95 \times 10 ⁻⁵ Pas	Water Viscosity	5 \times 10 ⁻⁴ Pas

The carbon graphite (i.e., the basic material from which the GDL is fabricated) is considered as a hydrophilic material with contact angle values ranging from 50° to 80° [20, 21]. To enhance the water removal property of the GDL, it is treated with a hydrophobic agent such as polytetrafluoroethylene (PTFE) which has contact angle values between 100° and 125° [20, 21]. However, in practice it is not possible to cover all the pores of the GDL with PTFE. The fraction of untreated pores is denoted by

f . The average contact angle of the GDL sample is calculated with respect to this fraction as suggested by [22]

$$\theta_c = \cos^{-1}[f \cos \theta_{HI} + (1 - f) \cos \theta_{HO}] \quad (1)$$

where θ_{HI} is the contact angle of the hydrophilic material (carbon graphite), and θ_{HO} is the contact angle of the hydrophobic agent (PTFE). The pore network developed for the E-TEK carbon cloth is initially considered as completely hydrophilic by assigning a contact angle value in the range of 50° to 80° for all of the pores. The contact angle of the $(1 - f)$ fraction of the pores is then randomly modified to a number between 100° to 125°.

Displacing algorithm

For displacing water inside the network, the following assumptions are made:

1. The fluids (water and air) are immiscible and water is considered to be incompressible.
2. Each pore can contain both fluids (water or air), but the throats can only pass one fluid in each time step.
3. The volume of the throat is considered to be zero. So, both fluids are assumed to be resided in the pores.
4. The pressure drop occurs at the throats and the flow rate in each throat is calculated based on Poiseuille law.

The algorithm for displacing fluids in the network is working based on effective pressures. For each fluid, in every pore, six effective pressures are defined. Each of the pressures is associated with six throats connected to that pore. This pressure is acting as the main driving force for the fluid to move through the network. The effective pressure is composed of two terms: the capillary pressure and a pressure correction term. The capillary pressure, P_c , is defined as the pressure difference between the two existing phases in the porous medium (liquid phase, P_l and gas phase, P_g):

$$P_c = P_g - P_l \quad (2)$$

In this study, the gauge pressure of the air is assumed to be zero. So the pressure of the liquid water can be considered as the capillary pressure of the system ($P_c = -P_l$). The capillary pressure obeys the Laplace equation, and thus is evaluated from

$$P_c = \frac{2\sigma \cos \theta}{r} \quad (3)$$

where, σ is the interfacial tension of the corresponding fluid, θ is the contact angle between the fluid and the medium, and r is the radius of the corresponding throat. Six capillary pressures of a pore are generally different from each other since the radii of the throats are different. However, the pressure correction term is unique for each pore. This term is proportional to the saturation of the corresponding phase in the pore and also the bulk pressure (or the pressure of the fluid reservoir):

$$P_{corr} \propto S \cdot P_{bulk} \quad (4)$$

Since the effective pressures are defined for each pore, every throat would have two effective pressures at its two ends. The flow rate inside the throat is calculated with respect to these effective pressures following the Poiseuille law

$$\Delta P = \frac{128\mu L Q}{\pi d^4} \quad (5)$$

Boundary conditions

It is assumed that the rate at which water is produced at the catalyst layer is constant. Thus, a constant flow rate is considered as the boundary condition in this model. In each time step, based on the effective pressures, a flow rate is calculated for every throat. The total flow rate in the system is the summation of the flow rate for each throat. In order to conserve the total mass in each time step, the total flow rate should be equal to the injection rate for each phase. If the total flow rate is less than the boundary condition, the bulk pressure increases to increase the flow rate. Thus, in each time step, the algorithm seeks and finds the proper bulk pressure to comply with the general conservation of mass which involves solving a series of nonlinear equations. For the imbibition process, in which a wetting fluid invades a nonwetting fluid in the medium, the capillary pressure helps the invading fluid. Thus, the bulk pressure is adjusting itself in order to control the rate of penetration. In this case, the bulk pressure values are usually small and sometimes negative. In contrast, for the drainage process, since the capillary pressure acts as a resistive force in the system, the bulk pressure increases to increase the effective pressure. Local mass conservation is also considered by adopting the following equation for the volume of the liquid water in each pores:

$$\frac{dV_l}{dt} + \sum_i Q_i = 0 \quad (6)$$

Then, the saturation for each pore is evaluated using the volume of the liquid and total volume of the pore:

$$S = \frac{V_l}{V_p} \quad (7)$$

Thus, in each time step, the bulk pressure is modified with respect to the inlet injection rate. Then, the effective pressures are calculated and the flow rate associated with each throat is evaluated. With respect to these flow rates, the saturation of each pore is updated using the equations 6 and 7. The model adopted in this study does not search for the most likely pore to be filled in the next time step. The criteria for invading a pore are determined with respect to the effective pressure of that pore and its adjacent pore. This would ensure a more realistic approach since in reality several pores could be invaded simultaneously depending on the Ca number. As for the lateral boundary conditions, the throats on the sides of the mesh are assumed to be dead-ended. The breakthrough condition is defined as when the average saturation of the last layer of the GDL reaches to $\%f$, i.e. for the sample with $f = 0.6$, when the saturation of the last layer reaches to $\%60$, the condition of breakthrough is achieved [19].

RESULTS AND DISCUSSION

The pore-network model is developed for E-TEK GDLs (carbon type A). The thickness of the single layer GDL is $400\mu m$ and the macroporous substrate (MPS) of the GDL with the average pore diameter of $2 < d_{avg} < 6\mu m$ is considered in the simulation.

Effect of pore size distribution

Park and Popov [19] showed that increasing the average pore diameter of the macroporous substrate has no significant effect on the cell potential at low current densities. However, as the current density increases, the performance of the cell will be better for the MPS with a larger pore diameter (considering that the PTFE loading has no effect on the pore size distribution). This is primarily due to the higher level of saturation for the sample with a smaller pore diameter.

In this work, the evolution of the saturation profile with time for three different pore diameters is presented. The results are presented in terms of dimensionless parameters including t^* and z^* which are dimensionless time and distance from the catalyst layer, i.e. $t^* = 1$ corresponds to the breakthrough condition and $z^* = 1$ is the interface of the GDL and gas channel. For the smallest pore diameter ($d = 2\mu m$), the water penetrates into the GDL and reaches to the gas channel more rapidly (Figure 1), while for the larger pore diameters ($d = 4, 6\mu m$), more time is required for water to occupy the same position (compare $t^* = 0.75$ in Figures 1, 2 and 3). This might be interpreted as desirable factor since if water droplets penetrate and reach to the gas channel faster,

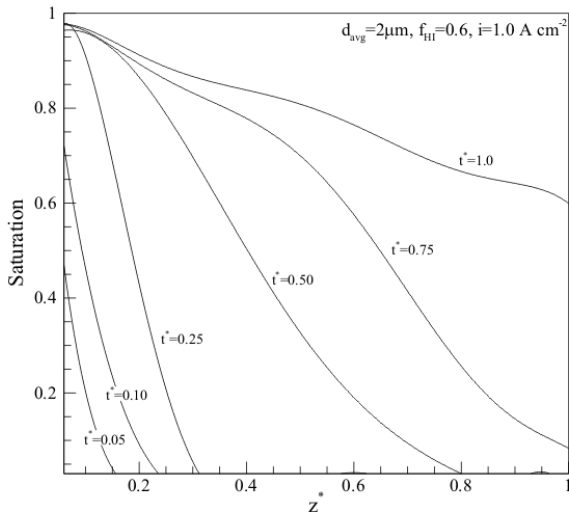


FIGURE 1. EVOLUTION OF SATURATION PROFILES WITH TIME ($d_{avg} = 2\mu m$).

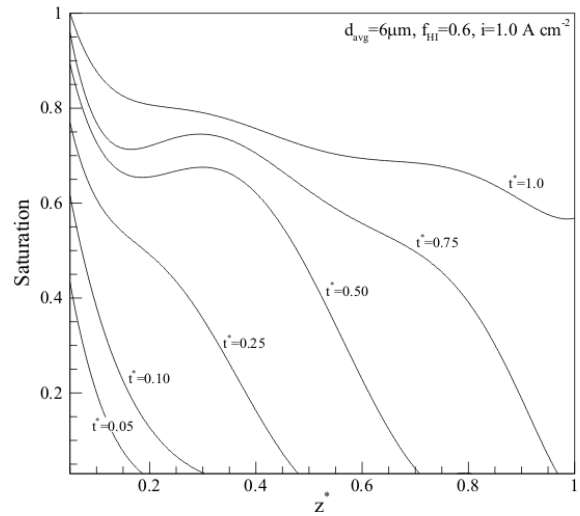


FIGURE 3. EVOLUTION OF SATURATION PROFILES WITH TIME ($d_{avg} = 6\mu m$).

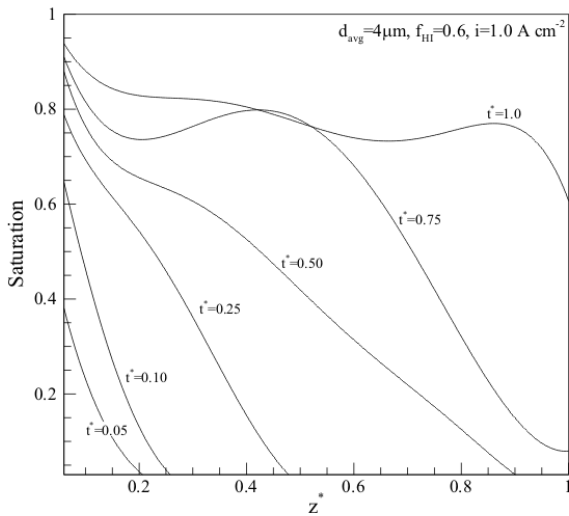


FIGURE 2. EVOLUTION OF SATURATION PROFILES WITH TIME ($d_{avg} = 4\mu m$).

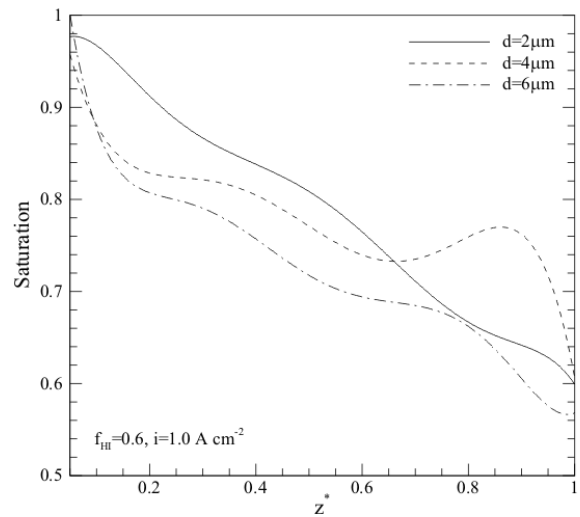


FIGURE 4. SATURATION PROFILES AT TIME OF BREAK-THROUGH.

they have more time for evaporation, and hence more liquid water would be removed from this interface. However, it appears that the saturation level at the catalyst layer at a particular time and the total saturation level are more important. For instance, consider the saturation level for $t^* = 0.1$ at $z^* = 0$. The satu-

ration level is higher for $d = 2\mu m$ indicating that liquid water covers the active area on the catalyst layer faster than the other cases. As the process progresses, liquid water distributes inside the sample quite uniformly for the smallest pore size. At the end of the process where the condition of breakthrough is achieved, the saturation level for the smallest pore size is higher in the ma-

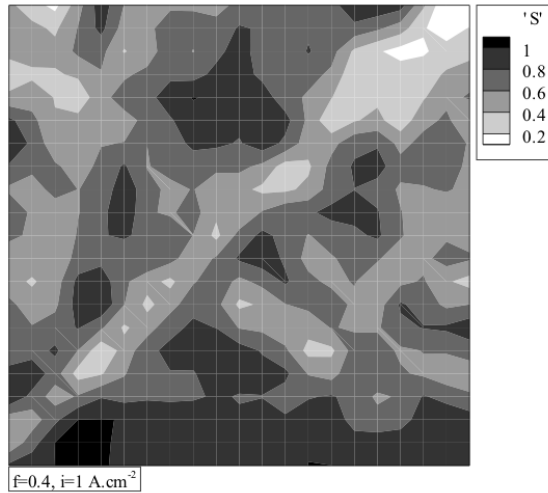


FIGURE 5. SATURATION PATTERN ($f = 0.4$).

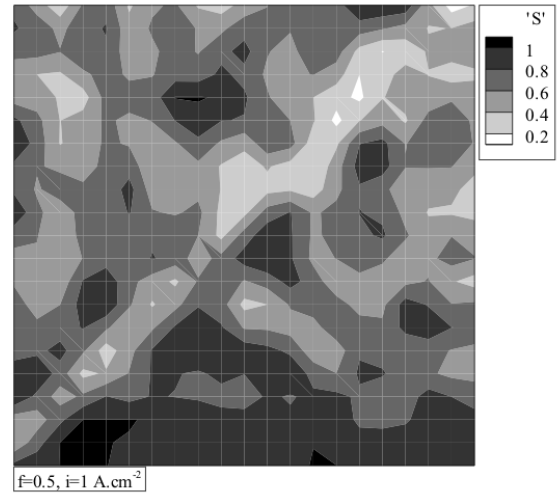


FIGURE 6. SATURATION PATTERN ($f = 0.5$)

majority sections of the GDL (Figure 4).

Effect of hydrophilic fraction

It is now a well-established fact that the GDL should be loaded with an optimum value of PTFE. Thus, a higher PTFE loading not necessarily leads to better water removal from the catalyst layer [14]. Using a 1D analytical model, Park and Popov [19] argued that this is due to reduction in the pore size distribution. As a result, they obtained the optimum pore size and hydrophilic fraction for the sample under study.

Chapuis et al. [10] also studied the effect of the contact angle on the evolution of the invasion pattern at the breakthrough condition using an invasion percolation model. They reported that the final configuration of the water inside the fibrous medium is getting closer to the stable displacement as the contact angle increases. Figures 5, 6 and 7 shows the liquid water pattern in the GDL at the breakthrough condition for three different hydrophilic fractions. For the lower hydrophilic fraction, the distribution followed the capillary fingering pattern (the existence of different independent highly-saturated regions supports this fact). As the hydrophilic content increases, water likes to form a more uniform configuration. For the case where $f = 0.6$, only three different independent regions of highly-saturated areas are distinguishable. In addition, the concentration of the liquid water near the catalyst layer is more significant for the sample with more hydrophilic contents (Figure 7).

Figures 8, 9 and 10 presents the evolution of the saturation distribution with time for different hydrophilic fractions. The agglomeration of liquid water occurs more rapidly on the surface of

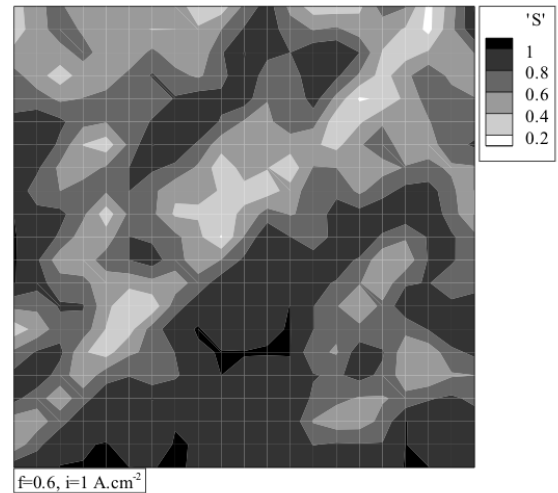


FIGURE 7. SATURATION PATTERN ($f = 0.6$)

the catalyst layer for the sample with a higher hydrophilic fraction (compare $t^* = 0.1$ for $f = 0.4, 0.5$ and 0.6). The oxygen transport is restricted at this region by the liquid water existing within the pores, which limits the current. In addition, at the time of breakthrough, the overall level of saturation across the GDL increases for higher f , as shown in Figure 11.

The saturation distribution obtained from the simulation is used with the analytical model proposed by Park and Popov [19]

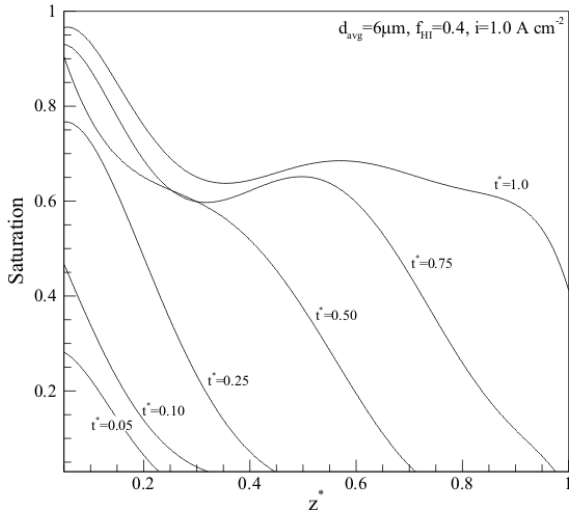


FIGURE 8. EVOLUTION OF SATURATION PROFILES WITH TIME ($f = 0.4$).

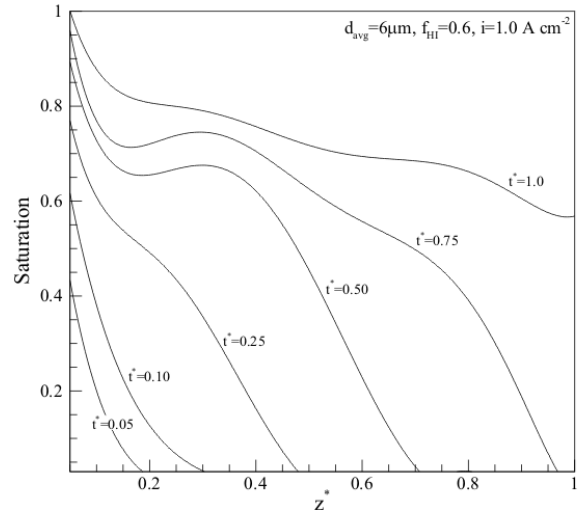


FIGURE 10. EVOLUTION OF SATURATION PROFILES WITH TIME ($f = 0.6$).

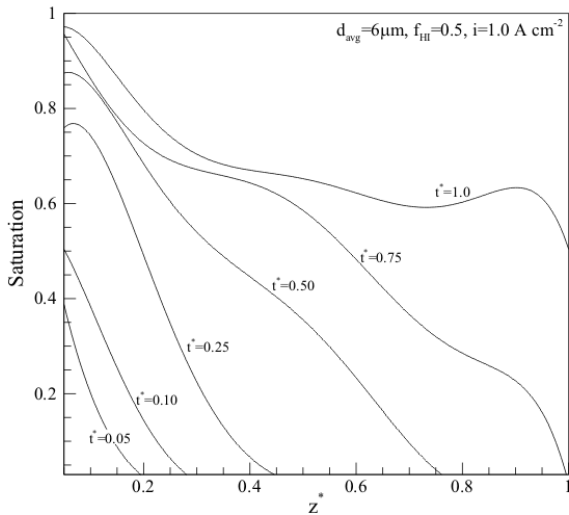


FIGURE 9. EVOLUTION OF SATURATION PROFILES WITH TIME ($f = 0.5$).

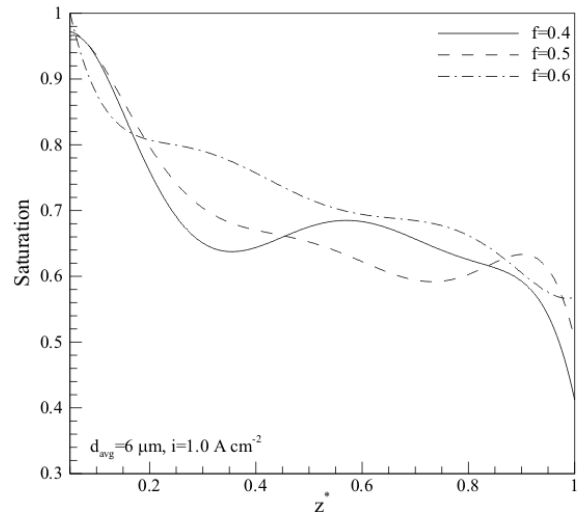


FIGURE 11. SATURATION PROFILES AT TIME OF BREAK-THROUGH.

to obtain the output voltage of the cell. Figure 12 compares the normalized cell voltage versus d_{avg} and the hydrophilic fraction f at $i = 1A/cm^2$. The maximum voltage is obtained where the GDL has the minimum hydrophilic fraction. As f increases, the voltage starts dropping. The performance of the GDL with a smaller pore diameter is worst compared to two larger diame-

ter cases ($d = 4$ and $6\mu m$). For a constant hydrophilic fraction ($f = 0.6$), the cell potential drops drastically as the average pore diameter becomes smaller. The figure suggests that the pore size distribution is a more important parameter than the hydrophilic fraction.

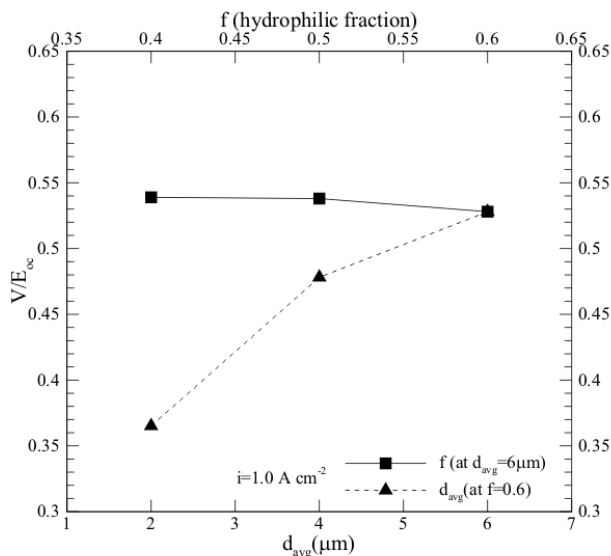


FIGURE 12. SATURATION PROFILES AT THE BREAK-THROUGH CONDITION.

CONCLUSION

In this work, transient response of the GDLs with different hydrophobic and structural properties investigated using a numerical model. Previous studies [15, 19] argued that the cell overpotential depends on the average liquid saturation inside the GDL at the steady-state condition. The numerical model presented here reproduced the saturation profiles at different time steps and showed that agglomeration of water droplets at the surface of the catalyst layer (CL) occurs faster for a GDL with a smaller pore size and a lower content of the hydrophobic agent. This transient analysis of the water flow inside the porous medium can be used as a tool to evaluate the performance of the medium in transporting liquid from the catalyst layer to the gas channel.

Acknowledgement

This work was supported by the Natural Science and Engineering Research Council (NSERC) of Canada. Financial support through the British Columbia Innovation Council (BCIC) scholarship is gratefully acknowledged.

REFERENCES

1. H. Li, Y. Tang, Z. Wang, Z. Shi, S. Wu, D. Song, J. Zhang, K. Fatih, J. Zhang and H. Wang, "A review of water flooding issues in the proton exchange membrane fuel cell," *J. Power Sources*, vol. 178, pp. 103-117, 2008.
2. S. Litster, D. Sinton and N. Djilali, "Ex situ visualization of liquid water transport in PEM fuel cell gas diffusion layers," *J. Power Sources*, vol. 154, pp. 95-105, 2006.
3. D. Natarajan and T. Van Nguyen, "Three-dimensional effects of liquid water flooding in the cathode of a PEM fuel cell," *J. Power Sources*, vol. 115, pp. 66-80, 2003.
4. A. Su, F. B. Weng, C. Y. Hsu and Y. M. Chen, "Studies on flooding in PEM fuel cell cathode channels," *Int J Hydrogen Energy*, vol. 31, pp. 1031-1039, 2006.
5. K. Tuber, D. Pcza and C. Hebling, "Visualization of water buildup in the cathode of a transparent PEM fuel cell," *J. Power Sources*, vol. 124, pp. 403-414, 2003.
6. F. B. Weng, A. Su, C. Y. Hsu and C. Y. Lee, "Study of water-flooding behaviour in cathode channel of a transparent proton-exchange membrane fuel cell," *J. Power Sources*, vol. 157, pp. 674-680, 2006.
7. T. Berning and N. Djilali, "Three-dimensional computational analysis of transport phenomena in a PEM fuel cell-a parametric study," *J. Power Sources*, vol. 124, pp. 440-452, 2003.
8. J. Baschuk and X. Li, "Modelling of polymer electrolyte membrane fuel cells with variable degrees of water flooding," *J. Power Sources*, vol. 86, pp. 181-196, 2000.
9. F. Barbir, *PEM Fuel Cells*. Springer, 2005.
10. O. Chapuis, M. Prat, M. Quintard, E. Chane-Kane, O. Guillet and N. Mayer, "Two-phase flow and evaporation in model fibrous media Application to the gas diffusion layer of PEM fuel cells," *J. Power Sources*, vol. 178, pp. 258-268, 2008.
11. J. T. Gostick, M. A. Ioannidis, M. W. Fowler and M. D. Pritzker, "Wettability and capillary behavior of fibrous gas diffusion media for polymer electrolyte membrane fuel cells," *J. Power Sources*, vol. 194, pp. 433-444, 2009.
12. J. T. Gostick, M. A. Ioannidis, M. W. Fowler and M. D. Pritzker, "Pore network modeling of fibrous gas diffusion layers for polymer electrolyte membrane fuel cells," *J. Power Sources*, vol. 173, pp. 277-290, 2007.
13. J. H. Nam and M. Kaviany, "Effective diffusivity and water-saturation distribution in single-and two-layer PEMFC diffusion medium," *Int. J. Heat Mass Transfer*, vol. 46, pp. 4595-4611, 2003.
14. S. Park, J. W. Lee and B. N. Popov, "Effect of PTFE content in microporous layer on water management in PEM fuel cells," *J. Power Sources*, vol. 177, pp. 457-463, 2008.
15. S. Park and B. N. Popov, "Effect of cathode GDL characteristics on mass transport in PEM fuel cells," *Fuel*, vol. 88, pp. 2068-2073, 2009.
16. P. K. Sinha, P. P. Mukherjee and C. Y. Wang, "Impact of GDL structure and wettability on water management in polymer electrolyte fuel cells," *Journal of Materials Chemistry*, vol. 17, pp. 3089-3103, 2007.

17. P. K. Sinha and C. Y. Wang, "Pore-network modeling of liquid water transport in gas diffusion layer of a polymer electrolyte fuel cell," *Electrochim. Acta*, vol. 52, pp. 7936-7945, 2007.
18. L. Jordan, A. Shukla, T. Behrsing, N. Avery, B. Muddle and M. Forsyth, "Diffusion layer parameters influencing optimal fuel cell performance," *J. Power Sources*, vol. 86, pp. 250-254, 2000.
19. S. Park and B. N. Popov, "Effect of hydrophobicity and pore geometry in cathode GDL on PEM fuel cell performance," *Electrochim. Acta*, vol. 54, pp. 3473-3479, 2009.
20. C. W. Extrand and Y. Kumagai, "Liquid drops on an inclined plane: the relation between contact angles, drop shape, and retentive force," *J. Colloid Interface Sci.*, vol. 170, pp. 515-521, 1995.
21. M. E. Schrader, "Ultrahigh vacuum techniques in the measurement of contact angles. IV. Water on graphite (0001)," *J. Phys. Chem.*, vol. 79, pp. 2508-2515, 1975.
22. J. Bear, *Dynamics of Fluids in Porous Media*. Dover Publications, 1988.
23. J. Koplik and T. Lasseeter, "One- and two-phase flow in network models of porous media," *Chemical Engineering Communications(Print)*, vol. 26, pp. 285-295, 1984.
24. J. Koplik and T. Lasseeter, "Two-phase flow in random network models of porous media," *Old SPE Journal*, vol. 25, pp. 89-100, 1985.
25. R. Lenormand, E. Touboul and C. Zarcone, "Numerical models and experiments on immiscible displacements in porous media," *J. Fluid Mech.*, vol. 189, pp. 165-187, 1988.